Maceral Control on the Hydrocarbon Generation Potential of Lacustrine Shales: A Case Study of the Chang 7 Member of the Triassic Yanchang Formation, Ordos Basin, North China

Bei Liu [1,2,3,*], Juan Teng [4] and Maria Mastalerz [5]

[1] State Key Laboratory of Shale Oil and Gas Enrichment Mechanisms and Effective Development, Beijing 100083, China
[2] Key Laboratory of Tectonics and Petroleum Resources of Ministry of Education, China University of Geosciences, Wuhan 430074, China
[3] School of Earth Resources, China University of Geosciences, Wuhan 430074, China
[4] College of Resources and Environment, Yangtze University, Wuhan 430100, China
[5] Indiana Geological and Water Survey, Indiana University, Bloomington, IN 47405-2208, USA
[*] Correspondence: liubei12@cug.edu.cn

Abstract: Organic matter (OM) type critically controls the hydrocarbon generation potential and organic pore development in black shales. However, maceral variation in lacustrine shales and its control on hydrocarbon generation potential and organic pore development are not yet well understood. In this study, 15 Chang 7 Member shale samples of the Yanchang Formation, Ordos Basin, were investigated with organic petrography, Rock-Eval pyrolysis, and a scanning electron microscope to study the maceral composition, hydrocarbon generation potential, and organic pores in this black shale succession. The results show that the studied shales are in the oil window (R_o~0.70%). OM belongs to Type I and Type III kerogen, as demonstrated by Rock-Eval pyrolysis. Macerals in the Chang 7 Member shales are composed of amorphous OM, alginite, sporinite, liptodetrinite, vitrinite, inertinite, and solid bitumen. Amorphous OM and alginite are major hydrocarbon-generating macerals, and their content determines the hydrocarbon potential of shales. Secondary organic pores were not observed in the studied Chang 7 Member shales due to either a low thermal maturity or a dominance of terrigenous OM. Maceral variation can affect the reliability of using Rock-Eval Tmax as a thermal maturity indicator. This study provides important insights into maceral control on hydrocarbon generation and organic pore development in black shales, calling for a critical evaluation of OM in black shale successions with organic petrography.

Keywords: maceral; hydrocarbon generation potential; organic pores; lacustrine shales; Yanchang Formation; Chang 7 Member

1. Introduction

Organic matter (OM) quantity and quality determine the hydrocarbon generation potential of organic-rich shales and are important parameters in both conventional and unconventional oil and gas systems [1–3]. The OM in black shales is heterogeneous and composed of different macerals when examined with a microscope [3–8]. These different macerals have varying origins and different hydrocarbon generation potentials. Documenting the OM type and its control on the hydrocarbon generation potential of black shales will provide important insights into petroleum source rock evaluation, as well as into shale oil and gas exploration and development.

Dispersed OM in black shales can be classified into five maceral groups based on reflectance, origin, morphology, texture, fluorescence, and other optical properties, with each group containing multiple macerals [2,4–8]. The liptinite group is derived from lipid materials and has the highest hydrocarbon generation potential among the five maceral

groups [9,10]. The vitrinite and inertinite groups are derived from terrigenous higher plants [11]. Vitrinite generally has a low oil potential but can generate some light hydrocarbons. In comparison, inertinite has almost no hydrocarbon generation potential, because it is burnt or oxidized before deposition [11]. Zooclasts, such as graptolites and chitinozoans, have a lower hydrocarbon generation potential than vitrinite because their reflectance values are generally higher than that of vitrinite. The reflectance of OM is a proxy for the aromaticity of its molecular structure. Secondary OM is generated during hydrocarbon generation of oil-prone liptinite macerals and can further generate hydrocarbons when reaching higher thermal maturities [2,7,8].

The OM in lacustrine shales is generally Type I kerogen, such as the Green River Formation oil shale [12]. OM in lacustrine shales with high hydrocarbon generation potential is dominated by alginite and/or amorphous organic matter ((AOM); also referred to as amorphinite, bituminite, or amorphous kerogen) [13–15]. However, lacustrine shales can be enriched in terrigenous OM during periods of high detrital input, which results in a low hydrocarbon generation potential. Shale samples from the same drill core can have significantly different hydrogen index (HI) values as determined by Rock-Eval pyrolysis [16].

The heterogeneity of OM composition may cause uncertainties in evaluating the hydrocarbon generation potential of lacustrine shales. The purpose of this paper is to study the hydrocarbon generation potential of lacustrine shales from a maceral perspective using the Chang 7 Member of the Triassic Yanchang Formation, Ordos Basin, as an example. The specific objectives are to (1) examine maceral compositions in the Chang 7 Member of the Yanchang Formation and (2) analyze the control on maceral variations on the hydrocarbon generation potential and organic pore development in lacustrine shales.

2. Geological Setting

The Ordos Basin, in the western North China Craton, is the second-largest onshore hydrocarbon-bearing basin in China [17]. It is composed of six primary tectonic units, including the Yimeng Uplift in the north, the Jinxi Fold Belt in the east, the Weibei Uplift in the south, the Western Thrust Belt and the Tianhuan Depression in the west, and the Yishan Slope in the center (Figure 1) [17–20]. During the Middle and Late Triassic, the collision of the North China Block and Yangtze Block created a large, inland freshwater lake basin [18,21].

The Middle to Upper Triassic Yanchang Formation was deposited from fluvial and deltaic environments to lacustrine environments. The Yanchang Formation is more than 1000 m thick and can be subdivided into 10 members, i.e., Chang 10 to Chang 1 Member from bottom to top based on lithology, fossil assemblages, and geophysical log characteristics (Figure 2) [22–24]. The Yanchang Formation constitutes a complete second-order transgressive–regressive cycle and consists of at least seven depositional sequences [25]. The Chang 7 Member was deposited in semi-deep to deep lake environments during a period of maximum expansion of the Yanchang Lake [26,27]. The Chang 7 Member is the major source rock for shale oil and tight oil in the Yanchang Formation and is characterized by black shales. The OM in the black shales of the Chang 7 Member has high hydrocarbon generation potential and is dominated by Type I and II kerogen. The Chang 7 Member is a shale oil interval and the Chang 6 Member is a tight oil interval; oil in both members is sourced from the Chang 7 Member black shales. The total tight oil and shale oil resources in the Chang 7 and Chang 6 Members are approximately 30×10^8 t [28]. By the end of 2018, the annual production of tight oil and shale oil from the Yanchang Formation was about 100×10^4 t [29].
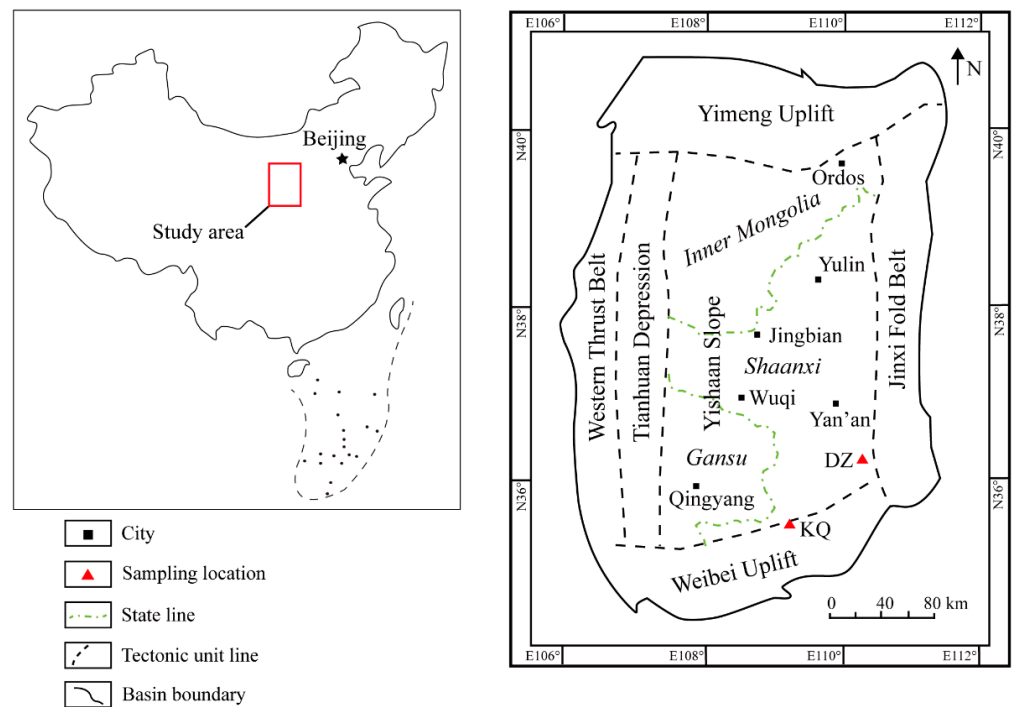
Figure 1. Map showing the tectonic units of the Ordos Basin and sampling locations. KQ = Kuquan section; DZ = Danzhou section.
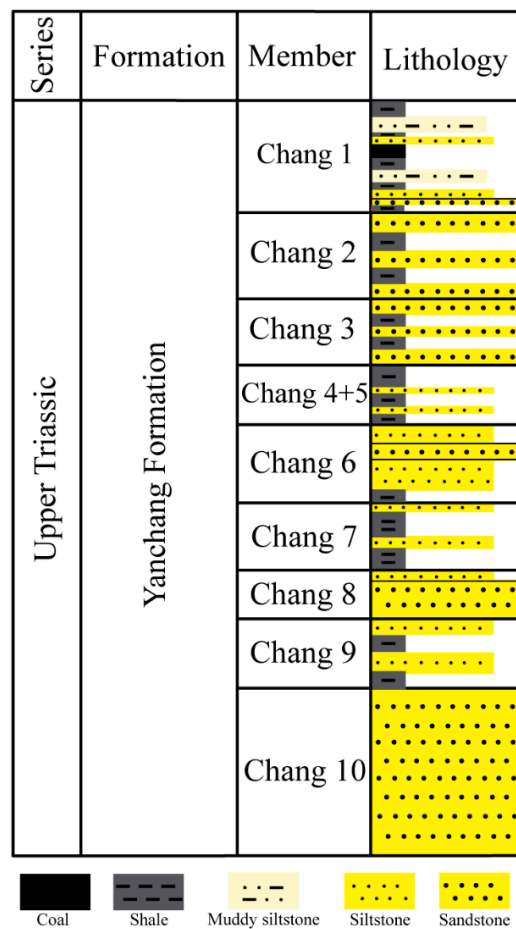
Figure 2. Generalized stratigraphy of the Triassic Yanchang Formation in the Ordos Basin. The thickness of different members is not to scale.

3. Samples and Analytical Methods

3.1. Samples

Fifteen shale samples from two outcrop sections (Figure 1) were collected to study OM content, maceral composition, and hydrocarbon generation potential of black shales belonging to the Chang 7 Member of the Triassic Yanchang Formation, Ordos Basin. The Kuquan section (KQ section) is in Yijun County, Tongchuan, Shaanxi, and the Danzhou section (DZ section) is in Yichuan County, Yan'an, Shaanxi. Samples were collected at the bottom of the Chang 7 Member with a sampling distance of approximately 1 m. Freshly exposed and hard samples without signs of weathering were collected in the field.

3.2. Analytical Methods

3.2.1. Total Organic Carbon Content

The total organic carbon (TOC) content of shale samples was analyzed with an ELEMENTRAC CS-i elemental analyzer. Shale samples were crushed into powders to pass through a 200-mesh sieve. Shale powders were pretreated with 10 wt.% HCl to dissolve carbonate minerals. Solid residues after acid treatment were analyzed with the LECO elemental analyzer.

3.2.2. Organic Petrography

Shale samples were crushed into rock chips to pass through a 20-mesh sieve. The chips were made into petrographic pellets with epoxy and hardener following standard coal petrography procedures [30]. A Leica DM2500 P microscope equipped with a Leica DFC 310 FX digital camera was used to investigate the organic petrographic characteristics of different macerals such as occurrence, color, fluorescence, size, and texture. Vitrinite reflectance (R_o) was measured with a Zeiss Photoscope III reflected-light microscope linked to a TIDAS PMT IV photometric system. Maceral composition of the studied shale samples was determined via point counting with more than 500 points.

3.2.3. Rock-Eval Pyrolysis

Rock-Eval pyrolysis of shale samples was conducted using a Rock-Eval 6 apparatus by Vinci Technologies. Powdered samples weighing 60 mg were introduced into the pyrolysis chamber in a N_2 atmosphere. The oven temperature was first increased to 300 °C and kept at 300 °C for 3 min. to vaporize volatile hydrocarbons in samples (S1). The temperature was then increased from 300 °C to 650 °C at a heating rate of 25 °C/min. S2 represents the yield of hydrocarbons generated through cracking of kerogen during pyrolysis. T_{max} corresponds to the temperature at the maximum hydrocarbon generation rate during pyrolysis. The hydrogen index (HI) was calculated as S2/TOC × 100, which represents the remaining hydrocarbon generation potential of kerogen.

3.2.4. Scanning Electron Microscopic Imaging

The pore characteristics of OM were investigated with a field-emission-scanning electron microscope (SEM) FEI Quanta 400 FEG. Shale samples were first cut into small blocks and then mechanically polished using successively finer-grit sandpapers. The mechanically polished samples were argon ion milled with a Gatan 600 DuoMill at 4 kV and a low incident angle (7.5°) [31–34].

4. Results

4.1. Organic Matter Content and Maceral Composition

The TOC content of the studied Chang 7 Member shale samples ranges from 0.30 to 33.15 wt.% (average 9.63 wt.%; Table 1). The KQ section samples have a much higher TOC content (average 21.86 wt.%) than the DZ section samples (average 1.48 wt.%). The average R_o of samples from the KQ section (R_o 0.70%) and the DZ section (R_o 0.71%) are very close (Table 1), suggesting oil-window maturity.

Table 1. Total organic carbon (TOC) content, vitrinite reflectance (R_o), and maceral composition (vol.%; on mineral-free basis) of the studied Chang 7 Member shale samples.

Sample	Location	TOC (wt.%)	R_o (%)	AOM	Alginite	Sporinite	Liptodetrinite	Vitrinite	Inertinite	Solid Bitumen
KQ-1	Kuquan section, Yijun County, Tongchuan, Shaanxi	12.48	0.69	60.6	24.2	1.5	1.5	1.5	1.5	9.1
KQ-2		22.80	0.67	62.1	14.7	0.0	2.1	2.1	1.1	17.9
KQ-3		19.39	0.71	54.9	23.2	0.0	1.2	1.2	1.2	18.3
KQ-4		21.62	0.67	68.8	17.2	0.0	1.1	3.2	1.1	8.6
KQ-5		21.73	0.74	67.5	21.2	1.3	1.3	0.7	1.3	6.6
KQ-6		33.15	0.69	78.6	4.2	0.4	4.2	0.7	0.7	11.2
Average		21.86	0.70	65.4	17.5	0.5	1.9	1.6	1.1	12.0
DZ-1	Danzhou section, Yichuan County, Yan'an, Shaanxi	0.31	0.72	0.0	0.0	11.1	22.2	44.4	22.2	0.0
DZ-2		0.30	0.72	0.0	0.0	25.0	25.0	37.5	12.5	0.0
DZ-3		0.30	0.71	0.0	0.0	10.5	26.3	52.6	10.5	0.0
DZ-4		0.55	0.70	10.5	0.0	10.5	26.3	42.1	10.5	0.0
DZ-5		0.72	0.71	0.0	0.0	7.1	21.4	50.0	21.4	0.0
DZ-6		1.76	0.68	0.0	0.0	5.9	23.5	47.1	23.5	0.0
DZ-7		3.70	0.70	0.0	0.0	3.7	7.4	77.8	11.1	0.0
DZ-8		2.14	0.71	0.0	0.0	6.7	20.0	66.7	6.7	0.0
DZ-9		3.54	0.71	0.0	0.0	4.0	8.0	80.0	8.0	0.0
Average		1.48	0.71	1.2	0.0	9.4	20.0	55.4	14.1	0.0

AOM = amorphous organic matter.

The OM in the studied Chang 7 Member shales consists of AOM, alginite, sporinite, liptodetrinite, vitrinite, inertinite, and solid bitumen (Table 1; Figure 3). AOM and alginite are the dominant macerals in samples from the KQ section, accounting for 65.4 vol.% and 17.5 vol.% of total OM, respectively. Vitrinite and inertinite content is low, with an average terrigenous OM content of 2.7 vol.%. Solid bitumen content is 12.0 vol.% on average. In comparison, OM in samples from the DZ section is dominated by vitrinite (average 55.4 vol.%) and inertinite (14.1 vol.%). AOM was only observed in one sample (DZ-4). Alginite and solid bitumen were not observed in the DZ section. It is noteworthy that in low-TOC samples from the DZ section, counting 500 points may be rather semiquantitative as far as OM is concerned. However, even without counting the points, it is obvious that vitrinite is the predominant maceral in this set of samples. The proportion of maceral in samples from the DZ section therefore reliably reflects their OM composition.

AOM occurs as layered structureless OM parallel to bedding (Figure 4A). Mineral particles are always mixed with AOM. Alginite occurs as distinct algal bodies and exhibits yellowish fluorescence (Figure 4C,D). Botryococcus was observed in places (Figure 4C). Vitrinite and inertinite are dispersed OM particles in the shale matrix (Figure 4E,F). Solid bitumen, a secondary product during thermal maturation, occurs between mineral grains (Figure 4G,H) and appears darker than vitrinite (Figure 4E).
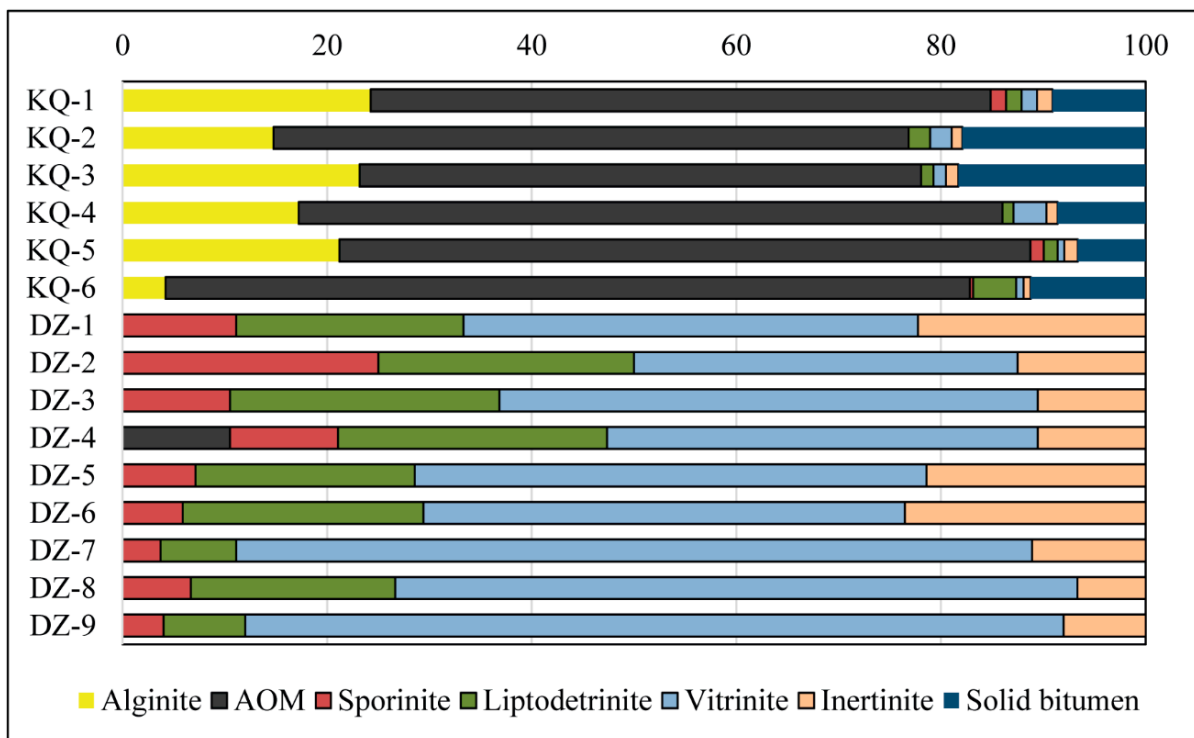
Figure 3. Maceral compositions of the studied Chang 7 Member shale samples determined by point counting. AOM = amorphous organic matter.
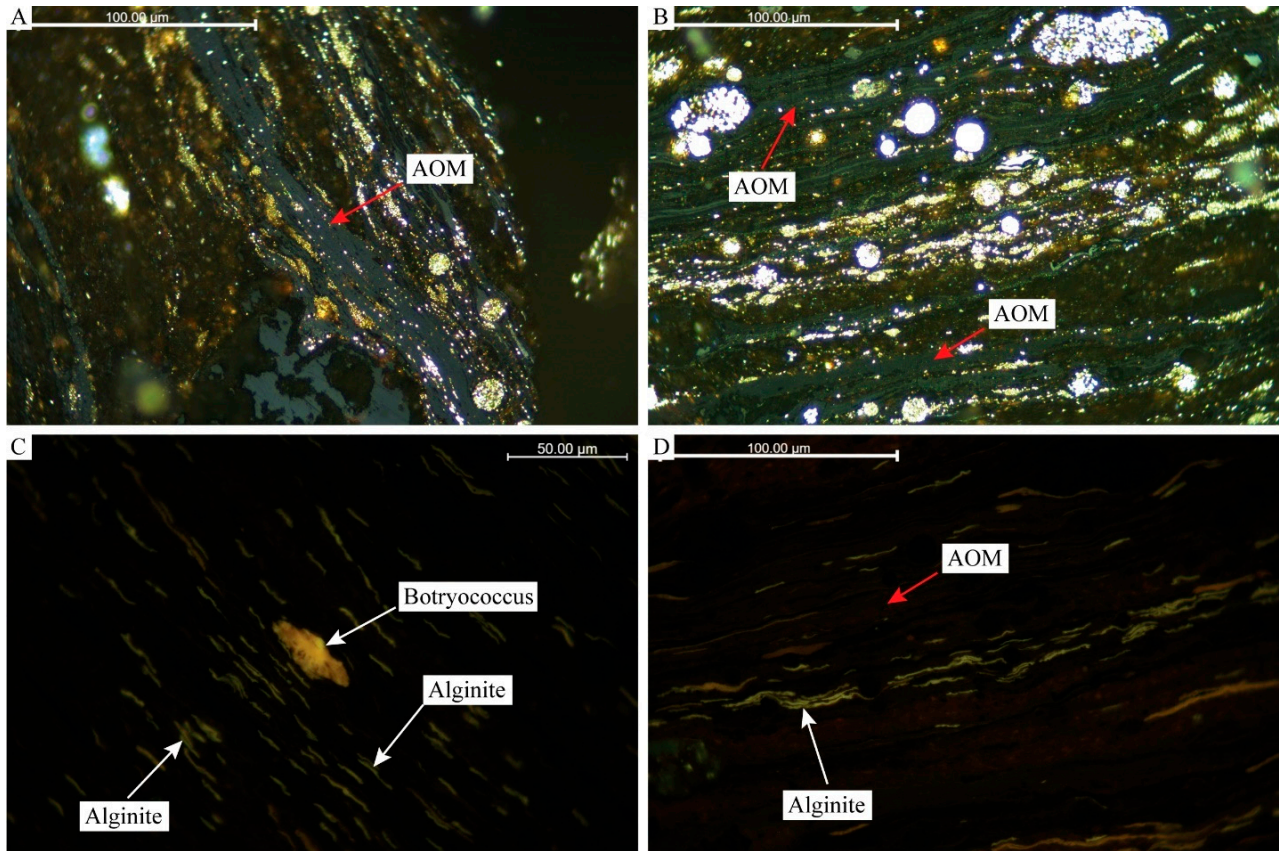
Figure 4. *Cont.*
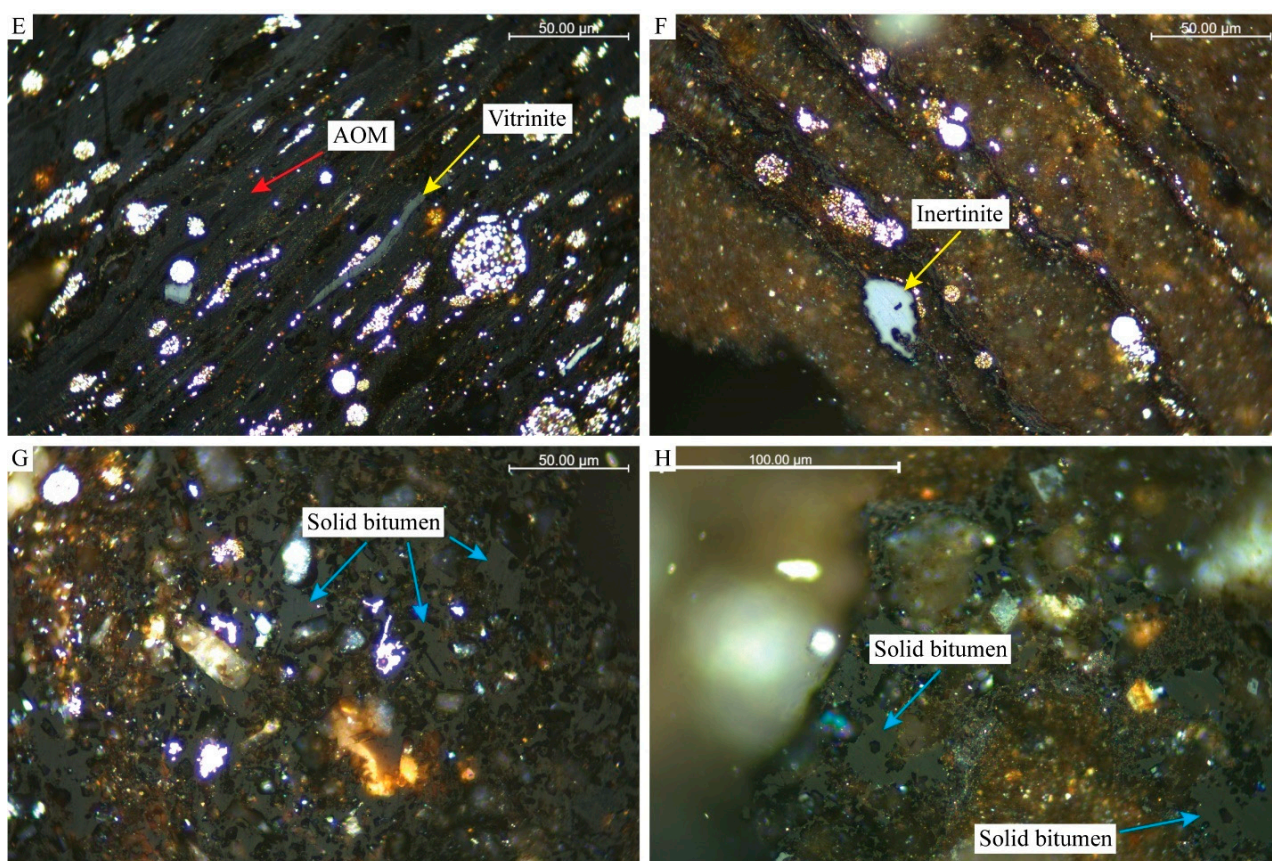
Figure 4. Photomicrographs of macerals in reflected white light and oil immersion (**A**,**B**,**E**–**H**) and in fluorescence mode (**C**,**D**) in the studied Chang 7 Member shale samples. (**A**,**B**) Amorphous organic matter (AOM). Note that AOM is mixed with fine mineral particles, especially pyrite. (**A**) Sample KQ-4. (**B**) Sample KQ-5. (**C**,**D**) Alginite. (**C**) A Botryococcus in the center. Abundant greenish yellow fluorescing algal bodies parallel to bedding. Sample KQ-2. (**D**) Intercalated greenish yellow fluorescing alginite and very weak brownish fluorescing AOM. Sample KQ-5. Panel D is the same view as panel B in fluorescence mode. (**E**) Vitrinite and AOM. Sample KQ-6. (**F**) Inertinite. Sample KQ-1. (**G**,**H**) Solid bitumen occurring between mineral grains. (**G**) Sample KQ-6. (**H**) Sample KQ-4.

4.2. Rock-Eval Pyrolysis

The HI values of samples from the KQ section range from 510 to 639 mg HC/g TOC, with an average value of 571 mg HC/g TOC. In comparison, the HI values of samples from the DZ section are much lower, ranging from 43 to 148 mg HC/g TOC, with an average value of 82 mg HC/g TOC (Table 2). The modified van Krevelen diagram shows that the OM in samples from the KQ section is Type I kerogen, whereas the OM in samples from the DZ section is a mixture of Type III and IV kerogen (Figure 5).

Table 2. Total organic carbon (TOC) content and Rock-Eval pyrolysis results of the studied Chang 7 Member shale samples.

Sample	TOC (wt.%)	S_1 (mg HC/g Sample)	S_2 (mg HC/g Sample)	S_3 (mg CO$_2$/g Sample)	T_{max} (°C)	HI (mg HC/g TOC)	OI (mg CO$_2$/g TOC)	R_o (%)	R_o-1	R_o-2	R_o-3
KQ-1	12.48	3.22	66.15	0.19	436	530	2	0.69	0.69	0.67	0.83
KQ-2	22.80	4.87	130.53	0.16	441	573	1	0.67	0.78	0.75	0.93
KQ-3	19.39	6.44	123.99	0.18	438	639	1	0.71	0.72	0.70	0.87

Sample	TOC (wt.%)	S_1 (mg HC/g Sample)	S_2 (mg HC/g Sample)	S_3 (mg CO_2/g Sample)	T_{max} (°C)	HI (mg HC/g TOC)	OI (mg CO_2/g TOC)	R_o (%)	R_o-1	R_o-2	R_o-3
KQ-4	21.62	3.4	110.25	0.61	433	510	3	0.67	0.63	0.63	0.78
KQ-5	21.73	7.09	131.43	0.38	436	605	2	0.74	0.69	0.67	0.83
KQ-6	33.15	8.55	188.54	0.72	435	569	2	0.69	0.67	0.66	0.82
Average	21.86	5.60	125.15	0.37	437	571	2	0.70	0.70	0.68	0.84
DZ-1	0.31	0.04	0.16	0.17	439	52	55	0.72	0.74	0.72	0.89
DZ-2	0.30	0.05	0.14	0.16	438	47	53	0.72	0.72	0.70	0.87
DZ-3	0.30	0.05	0.13	0.26	444	43	87	0.71	0.83	0.79	0.98
DZ-4	0.55	0.1	0.28	0.26	448	51	47	0.70	0.90	0.85	1.06
DZ-5	0.72	0.07	0.34	0.37	443	47	51	0.71	0.81	0.78	0.96
DZ-6	1.76	0.33	2.61	0.53	446	148	30	0.68	0.87	0.82	1.02
DZ-7	3.70	0.17	3.06	0.99	448	83	27	0.70	0.90	0.85	1.06
DZ-8	2.14	0.41	3.01	0.52	446	141	24	0.71	0.87	0.82	1.02
DZ-9	3.54	0.25	4.36	0.27	450	123	8	0.71	0.94	0.88	1.10
Average	1.48	0.16	1.57	0.39	445	82	42	0.71	0.84	0.80	1.00

S_1 = free hydrocarbons in shales; S_2 = generated hydrocarbons during pyrolysis; S_3 = generated CO_2; T_{max} = temperature of peak hydrocarbon generation; HI = hydrogen index; OI = oxygen index; HC = hydrocarbon. HI = S_2/TOC × 100; OI = S_3/TOC × 100. R_o-1: Calculated vitrinite reflectance (R_o) from T_{max} based on the empirical equation R_o = 0.018 × T_{max} − 7.16. R_o-2: Calculated vitrinite reflectance (R_o) from T_{max} based on the empirical equation R_o = 0.0151 × T_{max} − 5.9127. R_o-3: Calculated vitrinite reflectance (R_o) from T_{max} based on the empirical equation R_o = 0.01867 × T_{max} − 7.306.
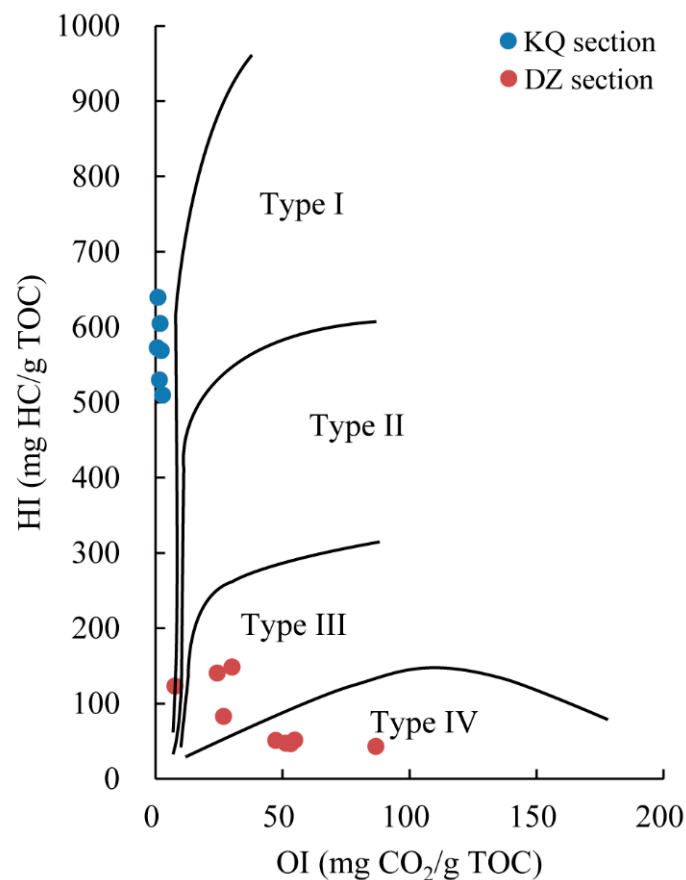
Figure 5. Modified van Krevelen diagram displaying kerogen types of the studied Chang 7 Member shales.

The T_{max} values of samples from the two sections are very close. The average T_{max} values of the KQ section and DZ section are 437 °C and 445 °C, respectively, which translate to R_o values of 0.70% and 0.84%, 0.68% and 0.80%, and 0.84% and 1.00%, respectively, based on the empirical equations of Jarvie et al. [35], Mastalerz et al. [36] and Laughrey [37] (Table 2). The average calculated R_o values (0.70% and 0.68%) of samples from the KQ section based on the empirical equations of Jarvie et al. [35] and Mastalerz et al. [36] are very close to the measured R_o (0.70%). However, all the calculated R_o values of samples from the DZ section are higher than the measured R_o (Table 2).

4.3. Organic Matter-Hosted Pores

OM-hosted pores were only observed in terrigenous OM, probably representing cellular pores in inertinite (Figure 6A,B). Pores in inertinite are mostly round (Figure 6). Other macerals such as AOM do not show pores in the studied Chang 7 Member shales (Figure 6C,D and Figure 7).
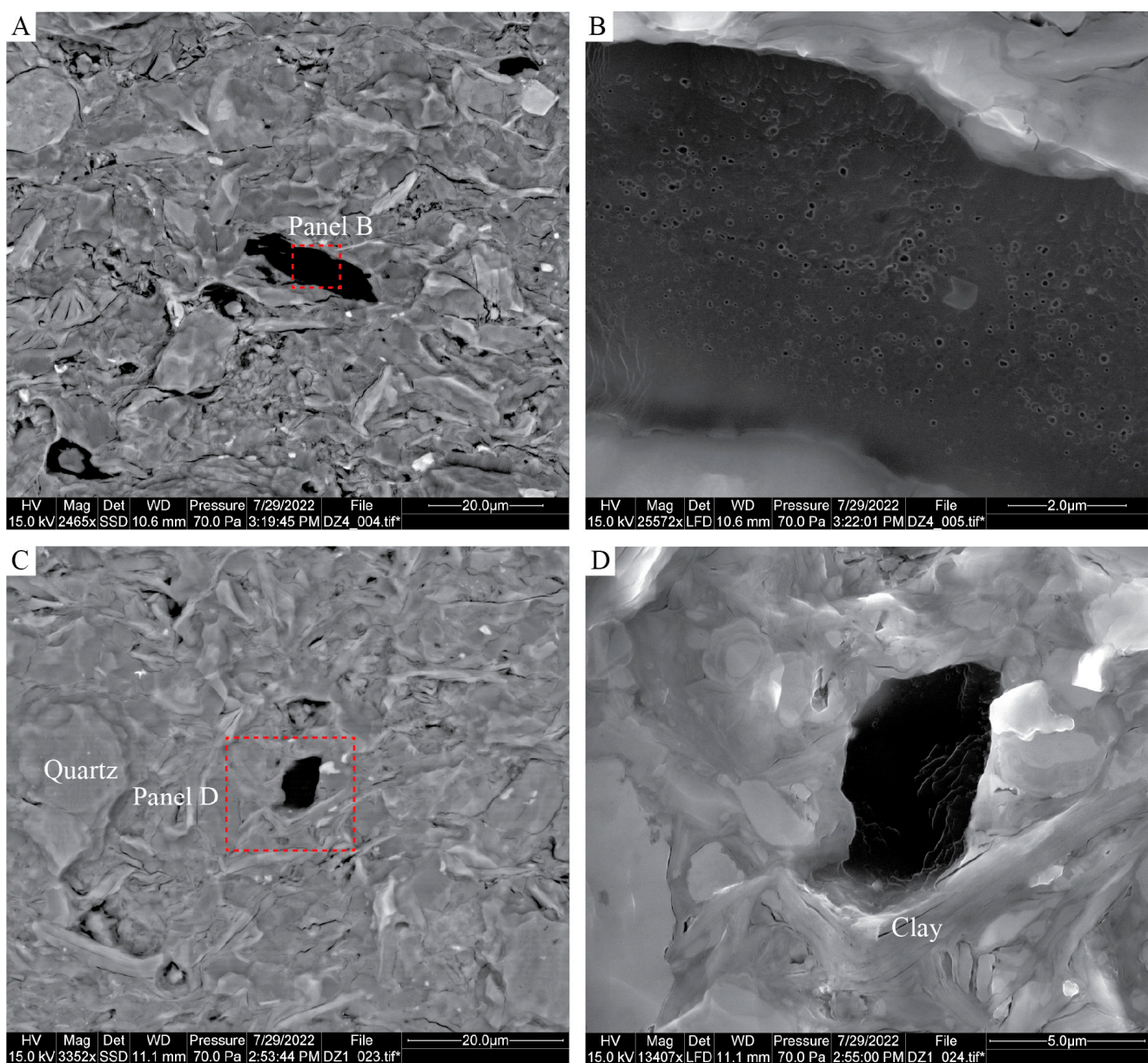
Figure 6. SEM images of terrigenous organic matter. (**A**,**B**) Inertinite with cellular pores, sample DZ-4. (**C**,**D**) Terrigenous organic matter without pores, sample DZ-1. Panels (**C**,**D**) are the enlarged views of the red dashed areas in panels (**A**,**C**), respectively.
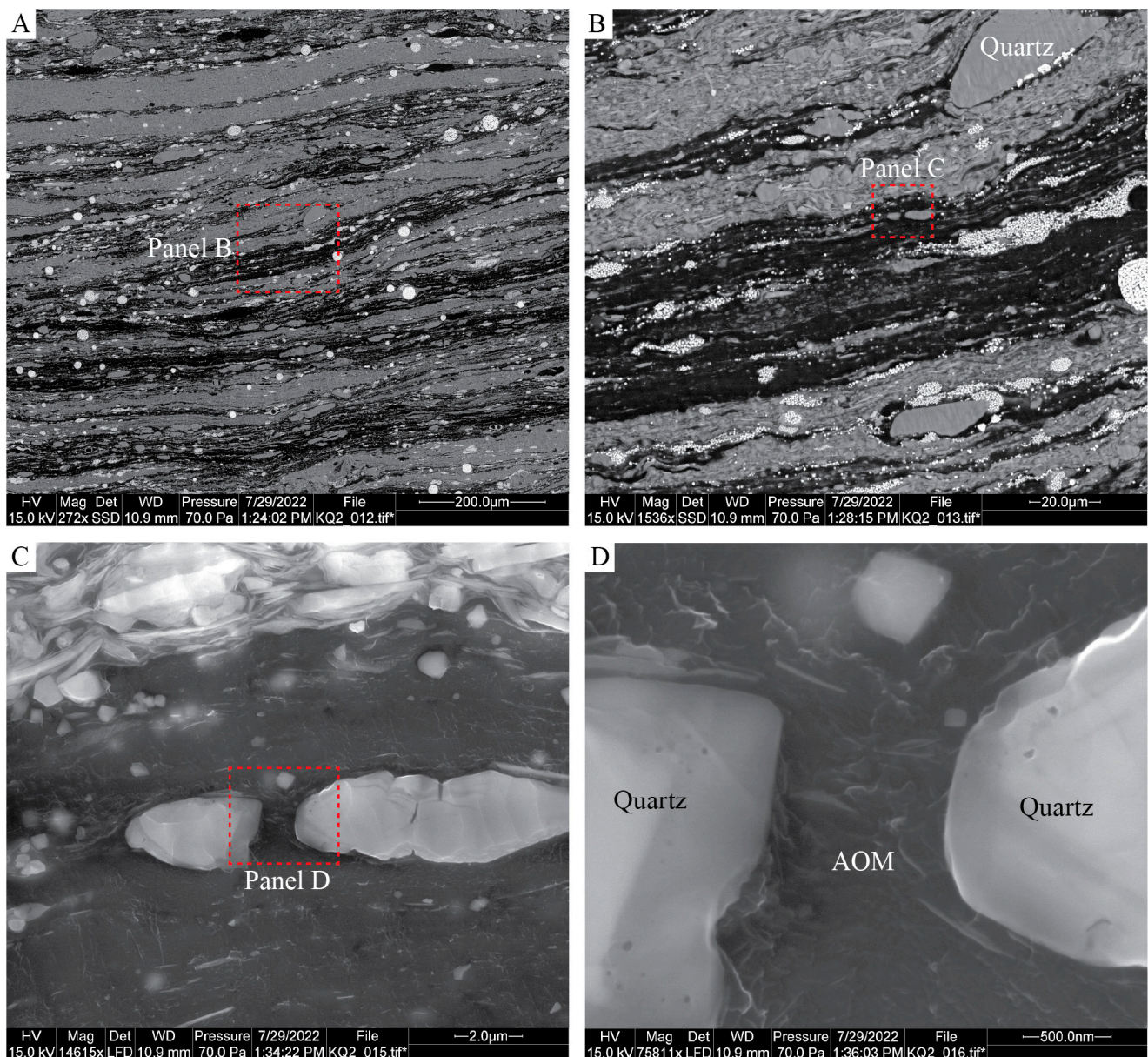
Figure 7. SEM images of amorphous organic matter (AOM), sample KQ-2. Note that AOM is mixed with mineral particles. Panels (**B**,**C**,**D**) are the close-up views of the red dashed areas in panels (**A**,**B**,**C**), respectively.

5. Discussion

5.1. Sedimentological Control on OM Content and Maceral Variation

OM accumulation in black shales is controlled by a combined effect of the terrigenous clastic supply, bottom-water redox conditions, and the paleo-productivity of the ocean surface, which applies to both marine and lacustrine shales [38–41]. OM-rich intervals generally occur near the maximum flooding surface within a sequence stratigraphic framework [38–41]. The Chang 7 Member black shales of the Yanchang Formation were deposited during maximum lake expansion [24,42,43]. Decreased clastic supply caused by lake transgression and oxygen deficiency of bottom waters resulted in the deposition of Chang 7 Member organic, rich black shales [24,42,44]. During deposition of the Chang 7 Member, the KQ section was located in a semi-deep to deep lake environment, whereas the DZ section was located in a prodelta to shallow lake environment [42,43]. The OM content of muddy sediments was diluted by terrigenous clastics in the DZ section, and

there is a significant input of terrigenous OM, as evidenced by high vitrinite and inertinite content in the DZ section (Table 1). In comparison, the OM content in the KQ section is high (average TOC >20 wt.%) due to significantly reduced input of detrital components; lacustrine OM, such as alginite and AOM, dominates the OM composition.

5.2. Maceral Control on Hydrocarbon Generation

Previous studies have identified AOM, alginite, sporinite, cutinite, liptodetrinite, vitrinite, inertinite, and solid bitumen (depending on thermal maturity) in the Chang 7 Member shales of the Yanchang Formation, Ordos Basin [16,45–47]. Alginite and AOM are major hydrocarbon-generating macerals in black shales [7,8,48,49]. The OM in samples from the KQ section is dominated by alginite and AOM (Table 1), which explains its high hydrocarbon generation potential (Figure 8A). AOM is derived from degraded phytoplanktons (mainly algae) and bacteria [15,50,51] and generally has a lower hydrocarbon potential than alginite, as demonstrated by micro-FTIR studies [15,48]. Alginite is generally characterized by abundant long, unbranched alkyl chains and little aromatic functional groups [15,48]. Some AOMs in the Chang 7 Member shales show very weak brownish fluorescence (Figure 4D), suggesting an algal origin and a degraded product. AOM in the Devonian New Albany Shale of the Illinois Basin also shows no or weak fluorescence [48].
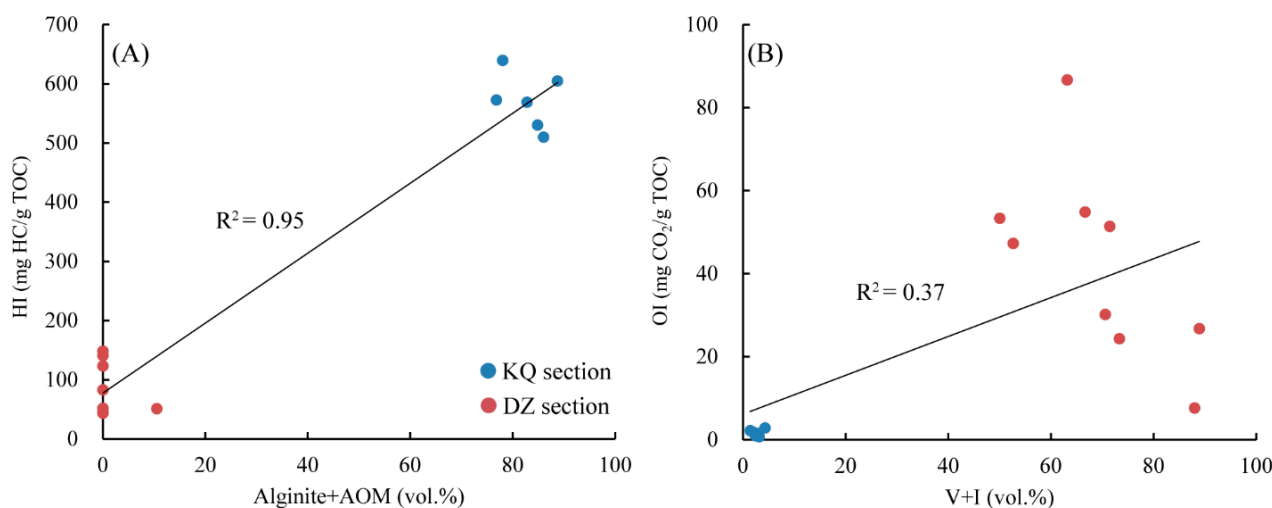
Figure 8. (**A**) Relationship between hydrogen index (HI) and alginite and amorphous organic matter (AOM) content; (**B**) relationship between oxygen index (OI) and vitrinite (V) and inertinite (I) content.

Terrigenous OM derived from land plants, especially vitrinite and inertinite, has low hydrocarbon generation potential and high O content in its macromolecular structure [52]. Inertinite is always oxidized or burned before burial [11]. Samples from the DZ section contain abundant terrigenous OM and are indeed characterized by high OI values (Figure 8B). Samples from the DZ section have a higher thermal maturity, but solid bitumen was not observed in the DZ section, also suggesting very limited hydrocarbon generation in the DZ section.

Rock-Eval Tmax has been used as an indicator of thermal maturity [35–37,53,54]. However, the reliability of Tmax can be influenced by many factors such as OM types, rock matrix, and experimental issues [53]. In this study, samples from both sections have a similar thermal maturity (R_o ~ 0.70%). The calculated R_o values (0.70% and 0.68%) of samples from the KQ section using the equations from Jarvie et al. [35] and Mastalerz et al. [36] are very close to the measured R_o (0.70%), but the calculated R_o values of samples from the DZ section (0.84% and 0.80%) are higher than the measured R_o (0.71%; Table 2). The reason could be that OM in the KQ section is mainly Type I kerogen, whereas the OM in the DZ section is Type III kerogen (Figure 5). Vitrinite pyrolysis has a higher activation energy and requires a higher temperature to generate hydrocarbons than liptinite [55,56], which results in a higher T_{max} of vitrinite-dominated OM than liptinite-dominated OM.

Therefore, when calculating vitrinite-reflectance-equivalent values, the equations from Jarvie et al. [35] and Mastalerz et al. [36] are best used for shales with Type I/II kerogen. Using these two equations in shales with Type III kerogen may overestimate the thermal maturity. Interestingly, R_o values calculated using the equation from Laughrey [37] are always higher than measured R_o values, even though this equation was developed based on 245 Woodford and Barnett shale samples. The reason is not clear, because the commonly used equation from Jarvie et al. [35] was based exclusively on Barnett shale samples.

5.3. Maceral Control on Organic Pore Development

Organic pores are important contributors to the pore network in black shales [8,31,57–62]. The development of organic pores in black shales is controlled by thermal maturity, maceral type, and mineralogy [7,8,59,63–68]. Organic pores were not observed in the KQ section due to low thermal maturity (R_o 0.70%). Teng et al. [19] reported that the lowest maturity when organic pores develop in the Chang 7 Member shales is R_o 0.77%, although they admit that organic pores could have developed between R_o 0.55% and 0.77%. Ko et al. [62] reported an abundance of organic pores in the Chang 7 Member shales with higher thermal maturities (BR_o 0.79–0.95%; R_o should be higher than BR_o in the oil window). Their samples are within the peak oil window and OM generates large amounts of bitumen, hydrocarbons, and organic pores as a result. In the studied oil-window-maturity shales (R_o ~ 0.70%), secondary organic pores could have developed in solid bitumen in the KQ section, but they were not observed, probably because of their scarcity.

No secondary organic pores were observed in the DZ section because of maceral type. The OM in samples from the DZ section is dominated by vitrinite and inertinite (Table 1), and both macerals have been reported not to develop secondary organic pores during thermal maturation [8,63]. Pores in inertinite make a limited contribution to total porosity because they are commonly filled with diagenetic minerals such as quartz and pyrite [8,63].

Pores here refer to those that are larger than 5 nm and can be detected under SEM. Previous studies have demonstrated that the OM in black shales possesses abundant micropores (<2 nm) and small mesopores (2–5 nm) characterized by low-pressure N_2 and CO_2 adsorption, even if no pores were observed under SEM [8,69].

6. Conclusions

Detailed organic petrographic and SEM analysis and Rock-Eval pyrolysis of OM in the Chang 7 Member shales of the Yanchang Formation, Ordos Basin, revealed maceral compositions and their control on hydrocarbon generation potential and organic pore development. The Chang 7 Member shales are OM rich, with an average TOC content of 9.63 wt.%. The HI can be as high as 639 mg HC/g TOC. The OM in the Chang 7 Member shales belongs to Type I and Type III kerogen. Macerals in the Chang 7 Member shales include AOM, alginite, sporinite, liptodetrinite, vitrinite, inertinite, and solid bitumen. AOM and alginite are major hydrocarbon-generating macerals, and their content determines the hydrocarbon generation potential of shales. Secondary organic pores did not develop due to either a low thermal maturity or a dominance of terrigenous OM.

References

1. Tissot, B.P.; Welte, D.H. *Petroleum Formation and Occurrence*, 2nd ed.; Springer: Berlin/Heidelberg, Germany, 1984.
2. Hackley, P.C.; Cardott, B.J. Application of organic petrography in North American shale petroleum systems: A review. *Int. J. Coal Geol.* **2016**, *163*, 8–51. [CrossRef]
3. Qiu, Z.; Zou, C. Controlling factors on the formation and distribution of "sweet-spot areas" of marine gas shales in South China and a preliminary discussion on unconventional petroleum sedimentology. *J. Asian Earth Sci.* **2020**, *194*, 103989. [CrossRef]
4. Potter, J.; Stasiuk, L.D.; Cameron, A.R. *A Petrographic Atlas of Canadian Coal Macerals and Dispersed Organic Matter*; Canadian Society for Coal Science and Organic Petrology—Geological Survey of Canada (Calgary)—Canmet Energy Technology Centre: Calgary, AB, Canada, 1998.
5. Stasiuk, L.D.; Burgess, J.; Thompson-Rizer, C.; Hutton, A.; Cardott, B. Status report on TSOP-ICCP dispersed organic matter classification working group. *Soc. Org. Petrol. Newsl.* **2002**, *19*, 14.
6. Flores, D.; Suárez-Ruiz, I. Organic petrology in the study of dispersed organic matter. In *The Role of Organic Petrology in the Exploration of Conventional and Unconventional Hydrocarbon Systems*; Suárez-Ruiz, I., Filho, J.G.M., Eds.; Bentham Science Publishers: Sharjah, United Arab Emirates, 2017; pp. 34–76.
7. Mastalerz, M.; Drobniak, A.; Stankiewicz, A.B. Origin, properties, and implications of solid bitumen in source-rock reservoirs: A review. *Int. J. Coal Geol.* **2018**, *195*, 14–36. [CrossRef]
8. Liu, B.; Mastalerz, M.; Schieber, J. SEM petrography of dispersed organic matter in black shales: A review. *Earth Sci. Rev.* **2022**, *224*, 103874. [CrossRef]
9. Peters, K.E.; Cassa, M.R. Applied source rock geochemistry. In *The Petroleum System—From Source to Trap*; AAPG Memoir; Magoon, L.B., Dow, W.G., Eds.; American Association of Petroleum Geologists (AAPG): Tulsa, OK, USA, 1994; Volume 60, pp. 93–120.
10. Pickel, W.; Kus, J.; Flores, D.; Kalaitzidis, S.; Christanis, K.; Cardott, B.J.; Misz-Kennan, M.; Rodrigues, S.; Hentschel, A.; Hamor-Vido, M.; et al. Classification of liptinite–ICCP System 1994. *Int. J. Coal Geol.* **2017**, *169*, 40–61. [CrossRef]
11. Taylor, G.H.; Teichmüller, M.; Davis, A.; Diessel, C.F.K.; Littke, R.; Robert, P. *Organic Petrology*; Gebrüder Borntraeger: Berlin, Germany; Stuttgart, Germany, 1998.
12. French, K.L.; Birdwell, J.E.; Berg, M.V. Biomarker similarities between the saline lacustrine Eocene Green River and the Paleoproterozoic Barney Creek Formations. *Geochim. Cosmochim. Acta* **2020**, *274*, 228–245. [CrossRef]
13. Thompson-Rizer, C.L. Optical description of amorphous kerogen in both thin sections and isolated kerogen preparations of Precambrian to Eocene shale samples. *Precambrian Res.* **1993**, *61*, 181–190. [CrossRef]
14. Kus, J.; Araujo, C.V.; Borrego, A.G.; Flores, D.; Hackley, P.C.; Hámor-Vidó, M.; Kalaitzidis, S.; Kommeren, C.J.; Kwiecińska, B.; Mastalerz, M.; et al. Identification of alginite and bituminite in rocks other than coal. 2006, 2009, and 2011 round robin exercises of the ICCP Identification of Dispersed Organic Matter Working Group. *Int. J. Coal Geol.* **2017**, *178*, 26–38. [CrossRef]
15. Teng, J.; Mastalerz, M.; Liu, B. Petrographic and chemical structure characteristics of amorphous organic matter in marine black shales: Insights from Pennsylvanian and Devonian black shales in the Illinois Basin. *Int. J. Coal Geol.* **2021**, *235*, 103676. [CrossRef]
16. Teng, J.; Deng, H.; Xia, Y.; Chen, W.; Fu, M. Controls of amorphous organic matter on the hydrocarbon generation potential of lacustrine shales: A case study on the Chang 7 Member of Yanchang Formation, Ordos Basin, North China. *Energy Fuels* **2021**, *35*, 5879–5888. [CrossRef]
17. Liu, K.; Liu, J.; Huang, X. Coupled stratigraphic and petroleum system modeling: Examples from the Ordos Basin, China. *AAPG Bull.* **2021**, *105*, 1–28. [CrossRef]
18. Zhao, M.; Behr, H.J.; Ahrendt, H.; Wemmer, K.; Ren, Z.; Zhao, Z. Thermal and tectonic history of the Ordos Basin, China: Evidence from apatite fission track analysis, vitrinite reflectance, and K-Ar dating. *AAPG Bull.* **1996**, *80*, 1110–1133.
19. Teng, J.; Deng, H.; Liu, B.; Chen, W.; Fu, M.; Xia, Y.; Yu, H. Insights of the pore system of lacustrine shales from immature to late mature with the aid of petrology, mineralogy and porosimetry: A case study of the Triassic Yanchang Formation of the Ordos Basin, North China. *J. Pet. Sci. Eng.* **2021**, *196*, 107631. [CrossRef]
20. Wang, J.; Li, X.; Liu, H.; Deng, X.; Wanyan, R. Depocenter migration of the Ordos Basin in the late Triassic and its controls on shale distribution. *Interpretation* **2017**, *5*, 81–98. [CrossRef]
21. Yang, Y.; Li, W.; Ma, L. Tectonic and stratigraphic controls of hydrocarbon systems in the Ordos basin: A multicycle cratonic basin in central China. *AAPG Bull.* **2005**, *89*, 255–269. [CrossRef]
22. Zhao, J.; Mountney, N.P.; Liu, C.; Qu, H.; Lin, J. Outcrop architecture of a fluvio-lacustrine succession: Upper Triassic Yanchang Formation, Ordos Basin, China. *Mar. Pet. Geol.* **2015**, *68*, 394–413. [CrossRef]
23. Xie, X. Provenance and sediment dispersal of the Triassic Yanchang Formation, southwest Ordos Basin, China, and its implications. *Sediment. Geol.* **2016**, *335*, 1–16. [CrossRef]
24. Zou, C.; Zhu, R.; Chen, Z.; Ogg, J.G.; Wu, S.; Dong, D.; Qiu, Z.; Wang, Y.; Wang, L.; Lin, S.; et al. Organic-matter-rich shales of China. *Earth Sci. Rev.* **2019**, *189*, 51–78. [CrossRef]
25. Zavala, C.; Liu, H.; Li, X.; Arcuri, M.; Di Meglio, M.; Zorzano, A.; Otharán, G.; Hao, B.; Wang, Y. Lacustrine sequence stratigraphy: New insights from the study of the Yanchang Formation (Middle-Late Triassic), Ordos Basin, China. In *The Ordos Basin: Sedimentological Research for Hydrocarbons Exploration*; Van Loon, T., Yang, R., Eds.; Elsevier: Amsterdam, The Netherlands, 2022; pp. 309–335.

26. Rowe, H.D.; Wang, X.; Fa, B.; Zhang, T.; Ruppel, S.C.; Milliken, K.; Loucks, R.G.; Shen, Y.; Zhang, J.; Liang, Q.; et al. Chemostratigraphic insights into fluvio-lacustrine deposition, Yanchang Formation, Upper Triassic, Ordos Basin, China. *Interpretation* **2017**, *5*, 149–165. [CrossRef]

27. Feng, C.; Sun, M.; Liu, C.; Deng, X.; Xue, Y.; Dong, L. Seismic sedimentary characteristics and filling structure of the Upper Triassic Yanchang Formation, Ordos Basin, China. *Interpretation* **2020**, *8*, 259–274. [CrossRef]

28. Yang, H.; Li, S.; Liu, X. Characteristics and resources prospects of tight oil and shale oil in Ordos Basin. *Acta Pet. Sin.* **2013**, *34*, 1–11, (In Chinese with English abstract).

29. Qiu, Z.; Zou, C. Unconventional petroleum sedimentology: Connotation and prospect. *Acta Sedimentol. Sin.* **2020**, *38*, 1–29, (In Chinese with English abstract).

30. *ASTM-D2797*; Standard Practice for Preparing Coal Samples for Microscopical Analysis by Reflected Light. ASTM International: West Conshohocken, PA, USA, 2015.

31. Schieber, J. Common themes in the formation and preservation of intrinsic porosity in shales and mudstones-illustrated with examples across the Phanerozoic. In Proceedings of the SPE Unconventional Gas Conference, Pittsburgh, PA, USA, 23–25; February, 2010. SPE Paper 132370.

32. Schieber, J. SEM observations on ion-milled samples of Devonian black shales from Indiana and New York: The petrographic context of multiple pore types. In *Electron Microscopy of Shale Hydrocarbon Reservoirs*; AAPG Memoir; Camp, W., Diaz, E., Wawak, B., Eds.; American Association of Petroleum Geologists (AAPG): Tulsa, OK, USA, 2013; Volume 102, pp. 153–171.

33. Schieber, J.; Lazar, R.; Bohacs, K.; Klimentidis, R.; Dumitrescu, M.; Ottmann, J. An SEM study of porosity in the Eagle Ford Shale of Texas—Pore types and porosity distribution in a depositional and sequence-stratigraphic Context. In *The Eagle Ford Shale: A Renaissance in U.S. Oil Production*; AAPG Memoir; Breyer, J.A., Ed.; American Association of Petroleum Geologists (AAPG): Tulsa, OK, USA, 2016; Volume 110, pp. 167–186.

34. Mastalerz, M.; Schieber, J. Effect of ion milling on the perceived maturity of shale samples: Implications for organic petrography and SEM analysis. *Int. J. Coal Geol.* **2017**, *183*, 110–119. [CrossRef]

35. Jarvie, D.M.; Claxton, B.L.; Henk, F.; Breyer, J.T. Oil and shale gas from the Barnett Shale, Ft. Worth Basin, Texas. In Proceedings of the AAPG Annual Meeting Program, Denver, CO, USA, 3–6 June 2001; Volume 10, p. A100.

36. Mastalerz, M.; Hampton, L.; Drobniak, A. Thermal alteration index (TAI), vitrinite reflectance, and Tmax through maturation. In Proceedings of the 32nd Annual Meeting of the Society for Organic Petrology, Yogyakarta, Java, Indonesia, 20–27 September 2015.

37. Laughrey, C.D. Introductory geochemistry for shale gas, condensate-rich shales and tight oil reservoirs. In Proceedings of the URTeC Annual Meeting Short Course, Denver, CO, USA, 27 August 2014; p. 325.

38. Dong, T.; Harris, N.B.; Ayranci, K. Relative sea-level cycles and organic matter accumulation in shales of the Middle and Upper Devonian Horn River Group, northeastern British Columbia, Canada: Insights into sediment flux, redox conditions, and bioproductivity. *GSA Bull.* **2018**, *130*, 859–880. [CrossRef]

39. Liu, B.; Schieber, J.; Mastalerz, M.; Teng, J. Organic matter content and type variation in the sequence stratigraphic context of the Upper Devonian New Albany Shale, Illinois Basin. *Sediment. Geol.* **2019**, *383*, 101–120. [CrossRef]

40. Zhang, K.; Liu, R.; Liu, Z. Sedimentary sequence evolution and organic matter accumulation characteristics of the Chang 8–Chang 7 members in the Upper Triassic Yanchang Formation, southwest Ordos Basin, central China. *J. Pet. Sci. Eng.* **2021**, *196*, 107751. [CrossRef]

41. Zhang, T.; Hu, S.; Bu, Q.; Bai, B.; Tao, S.; Chen, Y.; Pan, Z.; Lin, S.; Pang, Z.; Xu, W.; et al. Effects of lacustrine depositional sequences on organic matter enrichment in the Chang 7 Shale, Ordos Basin, China. *Mar. Pet. Geol.* **2021**, *124*, 104778. [CrossRef]

42. Yuan, X.; Lin, S.; Liu, Q.; Yao, J.; Wang, L.; Guo, H.; Deng, X.; Cheng, D. Lacustrine fine-grained sedimentary features and organic-rich shale distribution pattern: A case study of Chang 7 Member of Triassic Yanchang Formation in Ordos Basin, NW China. *Pet. Explor. Dev.* **2015**, *42*, 34–43. [CrossRef]

43. Chen, Y.; Zhu, Z.; Zhang, L. Control actions of sedimentary environments and sedimentation rates on lacustrine oil shale distribution, an example of the oil shale in the Upper Triassic Yanchang Formation, southeastern Ordos Basin (NW China). *Mar. Pet. Geol.* **2019**, *102*, 508–520. [CrossRef]

44. Yuan, W.; Liu, G.; Stebbins, A.; Xu, L.; Niu, X.; Luo, W.; Li, C. Reconstruction of redox conditions during deposition of organic-rich shales of the Upper Triassic Yanchang Formation, Ordos Basin, China. *Palaeogeogr. Palaeoclimatol. Palaeoecol.* **2017**, *486*, 158–170. [CrossRef]

45. Chen, Y.; Lin, S.; Bai, B.; Zhang, T.; Pang, Z.; Tao, S.; Hu, S. Effects of petroleum retention and migration within the Triassic Chang 7 Member of the Ordos Basin, China. *Int. J. Coal Geol.* **2020**, *225*, 103502. [CrossRef]

46. Xiao, L.; Li, Z.; Hou, Y.; Xu, L.; Wang, L.; Yang, Y. Characteristics of organic macerals and their influence on hydrocarbon generation and storage: A case study of continental shale of the Yanchang Formation from the Ordos Basin, China. *Geofluids* **2021**, *2021*, 5537154. [CrossRef]

47. Hackley, P.C.; Zhang, L.; Zhang, T. Organic petrology of peak oil maturity Triassic Yanchang Formation lacustrine mudrocks, Ordos Basin, China. *Interpretation* **2017**, *5*, SF211–SF223. [CrossRef]

48. Liu, B.; Schieber, J.; Mastalerz, M. Petrographic and micro-FTIR study of organic matter in the Upper Devonian New Albany Shale during thermal maturation: Implications for kerogen transformation. In *Mudstone Diagenesis: Research Perspectives for Shale Hydrocarbon Reservoirs, Seals, and Source Rocks*; AAPG Memoir; Camp, W., Milliken, K., Taylor, K., Fishman, N., Hackley, P., Macquaker, J., Eds.; American Association of Petroleum Geologists (AAPG): Tulsa, OK, USA, 2019; Volume 120, pp. 165–188.

49. Goodarzi, F.; Hosseininejad, S.; Pedersen, P.K.; Gentzis, T.; Sanei, H. Characterization of immature oil shales from the Cretaceous Second White Specks Formation in Saskatchewan and Manitoba, Canada. *Mar. Pet. Geol.* **2022**, *143*, 105774. [CrossRef]

50. Teichmüller, M.; Ottenjann, K. Art und diagenese von liptiniten und lipoiden stoffen in einem Erdölmuttergestein auf grund fluoroeszenzmikroskopischer Untersuchungen. *Erdöl Kohle Erdgas Petrochem.* **1977**, *30*, 387–398.

51. Liu, B.; Mastalerz, M.; Schieber, J.; Teng, J. Association of uranium with macerals in marine black shales: Insights from the Upper Devonian New Albany Shale, Illinois Basin. *Int. J. Coal Geol.* **2020**, *217*, 103351. [CrossRef]

52. Chen, Y.; Mastalerz, M.; Schimmelmann, A. Characterization of chemical functional groups in macerals across different coal ranks via micro-FTIR spectroscopy. *Int. J. Coal Geol.* **2012**, *104*, 22–33. [CrossRef]

53. Katz, B.J.; Lin, F. Consideration of the limitations of thermal maturity with respect to vitrinite reflectance, Tmax, and other proxies. *AAPG Bull.* **2021**, *105*, 695–720. [CrossRef]

54. Yang, S.; Horsfield, B. Critical review of the uncertainty of Tmax in revealing the thermal maturity of organic matter in sedimentary rocks. *Int. J. Coal Geol.* **2020**, *225*, 103500. [CrossRef]

55. Xie, K.; Zhang, Y.; Li, C.; Ling, D. Pyrolysis characteristics of macerals separated from a single coal and their artificial mixture. *Fuel* **1991**, *70*, 474–479. [CrossRef]

56. Jarvie, D.M.; Lundell, L.L. Amount, type, and kinetics of thermal transformation of organic matter in the Miocene Monterey Formation. In *The Monterey Formation: From Rocks to Molecules*; Caroline, M.I., Jürgen, R., Eds.; Columbia University Press: New York, NY, USA, 2001; pp. 268–295.

57. Loucks, R.G.; Reed, R.M.; Ruppel, S.C.; Hammes, U. Spectrum of pore types and networks in mudrocks and a descriptive classification for matrix-related mudrock pores. *AAPG Bull.* **2012**, *96*, 1071–1098. [CrossRef]

58. Loucks, R.G.; Reed, R.M.; Ruppel, S.C.; Jarvie, D.M. Morphology, genesis, and distribution of nanometer-scale pores in siliceous mudstones of the Mississippian Barnett Shale. *J. Sediment. Res.* **2009**, *79*, 848–861. [CrossRef]

59. Cardott, B.J.; Landis, C.R.; Curtis, M.E. Post-oil solid bitumen network in the Woodford Shale, USA—A potential primary migration pathway. *Int. J. Coal Geol.* **2015**, *139*, 106–113. [CrossRef]

60. Katz, B.J.; Arango, I. Organic porosity: A geochemist's view of the current state of understanding. *Org. Geochem.* **2018**, *123*, 1–16. [CrossRef]

61. Liu, B.; Wang, Y.; Tian, S.; Guo, Y.; Wang, L.; Yasin, Q.; Yang, J. Impact of thermal maturity on the diagenesis and porosity of lacustrine oil-prone shales: Insights from natural shale samples with thermal maturation in the oil generation window. *Int. J. Coal Geol.* **2022**, *261*, 104079. [CrossRef]

62. Ko, L.T.; Loucks, R.G.; Milliken, K.L.; Liang, Q.; Zhang, T.; Sun, X.; Hackley, P.C.; Ruppel, S.C.; Peng, S. Controls on pore types and pore-size distribution in the Upper Triassic Yanchang Formation, Ordos Basin, China: Implications for pore evolution models of lacustrine mudrocks. *Interpretation* **2017**, *5*, SF127–SF148. [CrossRef]

63. Liu, B.; Schieber, J.; Mastalerz, M. Combined SEM and reflected light petrography of organic matter in the New Albany Shale (Devonian-Mississippian) in the Illinois Basin: A perspective on organic pore development with thermal maturation. *Int. J. Coal Geol.* **2017**, *184*, 57–72. [CrossRef]

64. Ardakani, O.H.; Sanei, H.; Ghanizadeh, A.; Lavoie, D.; Chen, Z.; Clarkson, C.R. Do all fractions of organic matter contribute equally in shale porosity? A case study from Upper Ordovician Utica Shale, southern Quebec, Canada. *Mar. Pet. Geol.* **2018**, *92*, 794–808. [CrossRef]

65. Wu, Z.; He, S.; Han, Y.; Zhai, G.; He, X.; Zhou, Z. Effect of organic matter type and maturity on organic matter pore formation of transitional facies shales: A case study on Upper Permian Longtan and Dalong Shales in middle Yangtze region, China. *J. Earth Sci.* **2020**, *31*, 368–384. [CrossRef]

66. Chen, S.; Zhang, C.; Li, X.; Zhang, Y.; Wang, X. Simulation of methane adsorption in diverse organic pores in shale reservoirs with multi-period geological evolution. *Int. J. Coal Sci. Technol.* **2021**, *8*, 844–855. [CrossRef]

67. Fishman, N.S.; Hackley, P.C.; Lowers, H.A.; Hill, R.J.; Egenhoff, S.O.; Eberl, D.D.; Blum, A.E. The nature of porosity in organic-rich mudstones of the Upper Jurassic Kimmeridge Clay Formation, North Sea, offshore United Kingdom. *Int. J. Coal Geol.* **2012**, *103*, 32–50. [CrossRef]

68. Liu, B.; Teng, J.; Li, C.; Li, B.; Bie, S.; Wang, Y. The control of shale composition on the pore structure characteristics of lacustrine shales: A case study of the Chang 7 Member of the Triassic Yanchang Formation, Ordos Basin, North China. *Energies* **2022**, *15*, 8353. [CrossRef]

69. Liu, B.; Teng, J.; Mastalerz, M.; Schieber, J.; Schimmelmann, A.; Bish, D. Compositional control on shale pore structure characteristics across a maturation gradient: Insights from the Devonian New Albany Shale and Marcellus Shale in the eastern United States. *Energy Fuels* **2021**, *35*, 7913–7929. [CrossRef]